

1 **An energy-dependent earthquake**
2 **moment-frequency distribution**

3 Spassiani Ilaria^{†,*} and Marzocchi Warner[‡]

4 [†]Corresponding author. *Email address:* ilaria.spassiani@ingv.it

5 ^{*}Istituto Nazionale di Geofisica e Vulcanologia (INGV), Roma, Italy

6 [‡]The University of Naples Federico II, Naples, Italy

Submitted to BSSA

Abstract

The magnitude-frequency distribution (MFD) of many earthquake catalogs is well described by the Gutenberg-Richter (GR) law, or its tapered version (TGR). This distribution is usually extrapolated to any subsets of the space-time window covered by the catalog. However, some empirical observations and logical thoughts may raise doubts about the validity of this extrapolation. For example, according to the elastic rebound theory, we may assert that the probability of a strong shock to nucleate within a short time-interval in a small area \mathcal{A} just ruptured by another strong event, should be lower than that expected by GR (or TGR): a lot of energy has already been released, and it takes time to recover to the previous state. Here we put forward a space-time modification of the TGR, named TGRE (energy-dependent TGR), where the corner seismic moment becomes a time-varying energy function depending on: i) the conceivable strongest shock that may nucleate in \mathcal{A} ; ii) the time elapsed since the last strong earthquake resetting the elastic energy in \mathcal{A} to a residual value; iii) the rate of the energy recovering, linked to the recurrence time of the fault(s) involved. The model also verifies an invariance condition: for large space-time windows the occurrence of a strong shock doesn't affect significantly the whole elastic energy available, i.e., the TGRE becomes the TGR. The model is simple and rooted in clearly stated assumptions. To evaluate its reliability and applicability, we apply it to the Landers sequence in 1992. As expected by TGRE, we find that the MFD close to the fault system interested by the mainshock (Mw7.3) differs from that of earthquakes off-fault, showing a lower corner magnitude. We speculate that TGRE may be profitably used in operational earthquake forecasting, and explains the empirical observation that strongest aftershocks nucleate always outside the

32 mainshock fault.

33 Introduction

34 The Gutenberg-Richter (GR) law (Gutenberg and Richter (1944)) and its tapered
35 version (TGR) (Kagan (2002a,b)) are the most used magnitude-frequency distributions
36 (MFD) at quite different space-time windows, such as, for example, in operational
37 earthquake forecasting models (Jordan et al. (2011); Marzocchi et al. (2017); Omi
38 et al. (2018); Michael et al. (2019)). The validity of the (T)GR rests on the assumption
39 that the magnitude of an earthquake is independent from the past seismicity for any
40 dimension of the space-time window. Although this assumption seems appropriate
41 when looking at large spatiotemporal domains, its validity at small space-time scales
42 conflicts with some empirical findings, for which the largest triggered events occur
43 outside the fault of the strong triggering earthquake (van der Elst and Shaw (2015);
44 Stallone and Marzocchi (2019)).

45 Conceptually, this empirical observation could be explained in the framework of
46 the elastic rebound theory (Reid (1911)), for which one strong earthquake decreases
47 significantly the elastic energy available in the fault that generates the shock, and
48 it takes time to recover it. This means that the probability of a strong shock to
49 nucleate in the same area where another strong earthquake just occurred within a
50 short-time window, has to be lower than that predicted by the (T)GR law. Conversely,
51 if we consider a larger spatial scale, the occurrence of a single shock does not affect
52 significantly the elastic energy available in the area, so it is expected that the (T)GR
53 keeps holding. Besides the empirical evidence, we notice that the existence of a possible

54 variability of MFD stems from recent operational earthquake forecasting models (Field
55 et al. (2017a,b)), based on faults system which can produce reliable forecasts only when
56 the MFD is changed in space.

57 In this paper we put forward a space-time dependent model, which describes the
58 MFD of earthquakes that nucleate in small space-time areas, taking into consideration
59 the elastic energy released by the past seismicity in that area. The use of a small space-
60 time dimension marks the difference with very recent studies on a similar argument
61 (Marsan and Tan (2020)), and with past analyses on the definition of the maximum
62 magnitude expected in fixed (long) time windows (Zöller et al. (2013)). The model
63 introduces a time-varying corner seismic moment in the TGR law, which results from
64 the level of elastic energy that is currently available to be released in the space-time
65 area of interest. We name the model TGRE to explicitly reflect the dependence of
66 the MFD on the elastic energy available. In a nutshell, TGRE inhibits the nucleation
67 of large earthquakes in the area that just experienced a significant release of elastic
68 energy.

69 An alternative approach to model the space-time variability of the elastic energy
70 available is based on quantifying space-time variations of the b -value parameter in the
71 GR law (Gulia and Wiemer (2019)). For instance, a larger b -value diminishes the
72 probability of large earthquakes, but they still remain possible (e.g., if we keep fixed
73 the rate of M4+ earthquakes, increasing the b -value from 1.0 to 1.2 diminishes the
74 M7+ rate of a factor of about 4). Empirical evidence seems to show that this chance is
75 maybe lower, because large aftershocks nucleate almost exclusively in the outer regions
76 of the mainshock zone (van der Elst and Shaw (2015)). The model that we put forward

77 in this study is likely more suitable to explain such empirical evidence.

78 In the first part of this paper we describe the theoretical aspects of the model: we
79 explicitly derive its formulation and that of the time-varying corner seismic moment
80 with respect to which it is conditioned; we also discuss the stability conditions in
81 comparison with that of the classical GR model. In the second part we analyze the
82 Landers earthquake sequence, started on June 28, 1992, with a Mw7.3 event, with a
83 dual purpose: i) to find empirical evidence corroborating the existence of space-time
84 variability of the MFD; ii) to test if the proposed TGRE model better describes the
85 data than the space-time independent TGR model.

86 The energy-dependent MFD model (TGRE)

87 For the sake of mathematical simplicity, the TGRE is built in terms of seismic moment
88 instead of magnitude; the transition from one to the other can be easily made by
89 applying Kanamori (1977)'s relationship $m = \frac{2}{3} \log M - 10.73$, where M stays for
90 seismic moment (in dyne \times cm) and m for the corresponding moment magnitude.
91 Such a notation will be adopted in this paper hereafter; furthermore, owing to the
92 unambiguous relationship above, we will use the acronym MFD also for the seismic
93 moment-frequency distribution. The MFD Tapered Pareto GR (TGR) law introduced
94 by Kagan (2002a,b) reads:

$$\Phi_{TGR}(M) = \Phi_{GR}(M) \cdot \exp \left\{ \frac{M_{min} - M}{M_c} \right\}, \quad (1)$$

95 where $\Phi_{GR}(M) = \left(\frac{M}{M_{min}}\right)^{-\beta_k}$ is the GR-distribution, $\beta_k = \frac{2}{3}b$ -value, M_{min} is the com-
 96 pleteness threshold and M_c is the corner seismic moment, which is the value such that
 97 events with a higher seismic moment are less likely than what expected by the de-
 98 creasing exponential distribution. The tail of the GR law is therefore forced to decay
 99 stronger in the TGR model, the decay itself being controlled by the M_c value which
 100 is assumed as a fixed parameter, typically estimated through the maximum likelihood
 101 technique (Kagan and Schoenberg (2001)).

102 In this paper we introduce the TGRE model for earthquakes which nucleate inside
 103 an arbitray portion \mathcal{A} of the fault (the generalization to a volume is straightforward).
 104 The TGRE model relaxes the hypothesis that M_c is a fixed parameter, and it allows
 105 it to vary as a function of the amount of energy E currently available in \mathcal{A} , i.e.,
 106 $M_c \equiv M_c(E, t)$, where t is the time since the last earthquake which resets the energy in
 107 \mathcal{A} to a residual value. This function $M_c(E, t)$ has to consider the past earthquakes that
 108 nucleated in \mathcal{A} , as well as the earthquakes that involved \mathcal{A} in their rupture nucleated
 109 somewhere else (we use the term “participation” hereafter as in Parsons et al. (2018)).
 110 In this way, the TGRE model inhibits a second strong shock to nucleate in a small
 111 area that has been involved in a strong earthquake recently, but it does not prevent
 112 this area to participate to the rupture of another big event which may nucleate nearby,
 113 along the same fault(s) involved. It follows that the nucleation MFDs in two nearby
 114 small areas may be different, but still influenced by the reciprocal seismicity. For the
 115 sake of simplicity, hereafter we will omit to specify the dependence on t in the notation
 116 of $M_c(E)$.

117 We also constrain the model to respect a sort of “invariance condition”, i.e., the

118 TGRE turns back to the classical TGR at large spatiotemporal scales. This is to
 119 respect the evidence that, at large scales, the TGR law is well-validated. Of course,
 120 the specific choice of considering a time-varying corner seismic moment is not the only
 121 one possible to introduce an energy-dependence in the MFD, but it is justified in terms
 122 of easily practical use and testing; any other way of including a direct dependence on
 123 the energy can be proposed, provided that a higher complexity must be worth for a
 124 better reliability of the model, and coherence with previous pieces of evidence is needed.
 125 In the following subsections we define both the time-varying corner seismic moment
 126 $M_c(E)$, and the explicit distribution of the TGRE model.

127 **Time-varying corner seismic moment $M_c(E)$**

128 Here we propose a formulation of $M_c(E)$ based on two main concepts. First, the
 129 relevant quantities controlling the earthquake nucleation in \mathcal{A} are: the strongest earth-
 130 quake that can eventually nucleate in \mathcal{A} , and the most recent past earthquake which
 131 resets the available energy to the residual minimum value. Specifically, the elastic en-
 132 ergy in \mathcal{A} is reset to a residual minimum value by any earthquake that nucleates inside
 133 and generates a fractured area larger than \mathcal{A} . At the same time, the area is reset when
 134 it participates to a large earthquake which nucleates outside, but still involve \mathcal{A} . In
 135 other words, the resetting event must have a seismic moment $M \geq M_A$, where M_A is
 136 the seismic moment of an earthquake with area equal to \mathcal{A} . The latter's dimension
 137 plays therefore a direct role in the characterization of the relative resetting events. To
 138 determine if an event has involved this area, we check if at least part of \mathcal{A} falls in
 139 the CircleArea with the earthquake epicenter. The relative diameter (as well as M_A)

may be computed through any proper RuptureLength-MomentMagnitude relationship such as in Wells and Coppersmith (1994), Papazachos et al. (2004), or Allen and Hayes (2017).

Second, the elastic energy available in \mathcal{A} scales with times and it is related to M_c . In elasticity theory, $E \propto \sigma^2$, where E is the elastic energy accumulated as a consequence of the applied stress σ ; since the stress rate due to plate tectonics can be considered a constant value (that is, $\sigma \propto t$), it follows that $E \propto t^2$. The link between elastic energy available and seismic moment is instead more controversial. Here we assume that the radiated energy is a reliable proxy of the elastic energy drop, and that the radiated energy is proportional to the seismic moment, $E \propto M_c$; the latter holds only if the static stress drop of earthquakes is independent from the magnitude. These hypotheses are still matter of intense debate (Ide and Beroza (2001); Kanamori and Brodsky (2004); Oth et al. (2010)) and their validity is model-dependent (see e.g. Kanamori and Brodsky (2004)). However, we stress that a TGRE may be built adopting a different form of $M_c(E)$, which takes into account different hypotheses.

Going into the detail, we define the following parameters.

- a) M_c^* is the maximum corner seismic moment for earthquakes nucleating in \mathcal{A} . It is actually the corner seismic moment M_c adopted in the classical TGR distribution (1). We propose that M_c^* could be related, even though not necessarily, to the length of the longest fault included in the area: for instance, it can be obtained from any proper RuptureLength-MomentMagnitude relationship, such as those proposed in Wells and Coppersmith (1994), Papazachos et al. (2004), or Allen and Hayes (2017).

163 b) t_0 is the occurrence time of the earthquake which has reset the elastic energy in
 164 \mathcal{A} , i.e., the past earthquake at which \mathcal{A} participated.

165 c) $M_{c,0}^*$ sets the minimum value for the corner seismic moment which is achieved after
 166 the occurrence of a resetting earthquake in \mathcal{A} . In general, $M_{c,0}^* = \rho \cdot M_c^*$, where
 167 $\rho < 1$ indicates the fraction of elastic energy that is available after the resetting
 168 event. The value of ρ , or equivalently of $M_{c,0}^*$, may be either set theoretically,
 169 for instance by analyzing the stress rotation (Hardebeck and Okada (2018)), or
 170 empirically, by analyzing one or more stacked similar earthquake sequences.

171 d) ν is a parameter connected to the recurrence time of the longest fault involved
 172 in \mathcal{A} , and it controls the velocity of convergence to the maximum value M_c^* after
 173 a resetting event.

174 In “Application to real earthquakes: the Landers sequence”, subsection “Setting
 175 parameters and assumptions”, we describe some practical choices of these parameters.
 176 Still, we stress again that the choices are not prescriptive for the TGRE’s application;
 177 different $M_c(E)$ parameterizations, assumptions and parameters can be used.

178 According to the above concepts and definitions, we define the time-varying energy
 179 function as

$$M_c(E) = M_{c,0}^* + (M_c^* - M_{c,0}^*) [\nu(t - t_0)]^\alpha \quad (2)$$

180 bounded to the values $(t - t_0) \leq \frac{1}{\nu}$, which translates in $(t - t_0) \leq \tau$ when the coefficient
 181 of variation of the interevent times between consecutive earthquakes (CoV) is zero, i.e.,
 182 τ is the recurrence time between earthquakes. This restriction guarantees indeed that
 183 $M_c(E) \in [M_{c,0}^*, M_c^*]$ when $(t - t_0) \in [0, \tau]$, a requirement that is deducible from the

184 argument above. The dependence on time of the corner seismic moment is therefore
 185 expressed with respect to the time elapsed since the resetting event, and the seismic
 186 moments multiplication term allows us to account for the energy reloading process;
 187 while, $M_{c,0}^*$ is added to ensure that the available energy will not fall below its minimum
 188 value, even immediatly after the resetting event, that is, when $t - t_0 \sim 0$. In this paper,
 189 according to the proportionality between elastic energy and seismic moment, we set
 190 $\alpha = 2$ ($\alpha = 1$ if the seismic moment is assumed to increase linearly with time).

191 The temporal trend of $M_c(E)$, as well as its sensitivity to the parameters, can be
 192 observed in Fig. 1, whose plots are obtained by considering two parameters among
 193 $(M_c^*, M_{c,0}^*, \nu)$ fixed, the third varying; for an easier interpretation, we also display
 194 magnitude values instead of seismic moments. An overall increasing trend is shown
 195 in all the plots. As the intuition suggests, the time-varying corner seismic moment
 196 approaches more rapidly its maximum when ν becomes larger: the lower the recurrence
 197 time of the fault, the faster M_c^* can be reached. The increasing velocity of $M_c(E)$ is
 198 also faster as M_c^* is higher, whereas it does not change with $M_{c,0}^*$. This is because the
 199 influence of the latter on the taper's trend can be appreciated only within a short-
 200 time interval since the resetting event (less than 1 year in our example), being $M_c(E)$
 201 controlled mainly by M_c^* and ν at just larger scales: that's why the x -axes in plot *c*)
 202 are cut at 1 year after the reset, otherwise the difference would not have been visible.
 203 When focusing on the entire time window, we observe instead that the influence of ν
 204 and M_c^* on $M_c(E)$ is a bit stronger. However, Fig. 2 highlights that in the short-term,
 205 the time-varying corner seismic moment does not substantially depend on these two
 206 values.

207 To be thorough, we add that $M_c(E)$ could be also interpreted as a random variable
 208 whose distribution takes the cue from the stress level adopted in the stress release
 209 model (Vere-Jones (1978, 1988); Wang et al. (1991); Zheng and Vere-Jones (1991);
 210 Xiaogu and Vere-Jones (1994)). In fact, $M_c(E)$ could consist in a deterministic term
 211 of accumulated energy, linked to the elapsed time since the resetting event, and a
 212 stochastic term of energy released by each single past earthquake, which is distributed
 213 according to TGR. Nevertheless, so as to gain in easily applicability and reliability
 214 testing, we assume here that $M_c(E)$ is a deterministic function of time, as defined
 215 in (2).

216 **The mathematical description of the TGRE model**

217 The TGRE model we propose for earthquake seismic moments is simply obtained by
 218 including the time-varying corner seismic moment $M_c(E)$ previously derived, into the
 219 TGR cumulative distribution (1), i.e.,

$$\Phi_{TGRE}(M) = \left(\frac{M}{M_{min}} \right)^{-\beta_k} \exp \left\{ \frac{M_{min} - M}{M_c(E)} \right\}, \quad (3)$$

220 where $M_c(E) \in [M_{c,0}^*, M_c^*]$ is defined in (2) with $\alpha = 2$. Fig. 3 shows $\Phi_{TGRE}(M)$ as a
 221 function of $M_c(E)$.

222 If we consider a large spatial domain composed by many faults, and many cells \mathcal{A} ,
 223 the occurrence of one or a few large earthquakes may reset only a limited number of cells
 224 \mathcal{A} . This means that for the whole large spatial domain, $M_c(E) \equiv M_c^*$, acknowledging
 225 the spatial invariance condition. The temporal invariance condition is instead satisfied

226 by construction in fact, equation (2) gives M_c^* for $t - t_0 \rightarrow \tau$.

227 One obvious application of the TGRE model is in operational earthquake forecasting
 228 (OEF; Jordan et al. (2011)). It is expected to solve the main conundrum of existing
 229 OEF models (Marzocchi et al. (2017); Omi et al. (2018); Michael et al. (2019)), for
 230 which the probability of a large aftershock is exactly where the mainshock occurred.
 231 For example, the ETAS-TGRE (i.e., ETAS with TGRE) rate would be

$$\lambda(t, x, y, M | \mathcal{H}_t) = \left[\lambda_0(x, y) + \sum_{\{i|t_i < t\}} \lambda_{tr}(t - t_i, x - x_i, y - y_i; M_i) \right] p_{TGRE}(M | M_c(E)), \quad (4)$$

232 where \mathcal{H}_t is the past history up to time t , i.e., the past earthquakes $\{(t_i, x_i, y_i, M_i); t_i <$
 233 $t\}$; $\lambda_0(x, y)$ is the rate of the background events; $\lambda_{tr}(t - t_i, x - x_i, y - y_i; M_i)$ is the rate
 234 of the triggered events; $p_{TGRE}(M | M_c(E))$ is the TGRE probability density function
 235 for the seismic moment that is calculated in x, y at the time t ; finally, $M_c(E) \equiv$
 236 $M_c(E, x, y, s)$ is linked to the elastic energy available in x, y after a time s since the
 237 last resetting earthquake. In this framework, the TGRE may be applied to both the
 238 background and triggered earthquakes as in the classical ETAS model.

239 In the ETAS-TGRE setting, it is also interesting to investigate how the shift of
 240 the TGRE taper influences the computation of the branching ratio, which we recall
 241 being the average number of aftershocks triggered by an arbitrary event (Zhuang et al.
 242 (2012)). As for the TGR law, the branching ratio of the TGRE model can be derived

243 as

$$\eta_{TGRE} = \kappa + \kappa\alpha_k e^{\frac{M_{min}}{M_c(E)}} \left(\frac{M_{min}}{M_c(E)} \right)^{\beta_k - \alpha_k} \Gamma \left(-\beta_k + \alpha_k, \frac{M_{min}}{M_c(E)} \right), \quad (5)$$

244 where $\Gamma(s, t) = \int_t^\infty x^{s-1} e^{-x} dx$ is the upper incomplete Gamma function (Bateman
 245 (1953); Temme (1996); Spassiani (2020)), and κ, α_k are the parameters of the produc-
 246 tivity law $\varrho(\cdot)$ expressed in terms of the seismic moment through Kanamori (1977)'s
 247 relationship, i.e., $\varrho(M) = \kappa \left(\frac{M}{M_{min}} \right)^{\alpha_k}$. In Fig. 4 we show that η_{TGRE} increases with
 248 the time-varying corner seismic moment $M_c(E)$, indicating that if the taper moves
 249 to the left as a consequence of a great amount of energy just released, the average
 250 number of aftershocks triggered by a generic event is reduced: in fact, an event with
 251 a lower seismic moment will generate a lower number of aftershocks. The plot shows
 252 that the increasing behavior is faster as the difference $\beta_k - \alpha_k$ is lower: in the case
 253 of the classical ETAS-GR it has to be $\beta_k > \alpha_k$ for the process not to explode, but
 254 this condition becomes unnecessary for the ETAS-TGRE model, so as for ETAS-TGR
 255 (Spassiani (2020)). As usual, the stability of the ETAS-TGRE process is guaranteed
 256 by imposing $\eta_{TGRE} < 1$. Since this branching ratio increases with the corner seismic
 257 moment, we have that $\eta_{TGR} < 1$ is a sufficient condition for the stability of the ETAS-
 258 TGRE process, in fact, $M_c(E)$ assumes its maximum in M_c^* . We also stress that, when
 259 $\beta_k > \alpha_k$ it holds $\eta_{TGRE} < \eta_{GR}$, therefore in this case our model's stability conditions
 260 are less restrictive than those of ETAS-GR.

261 Application to real earthquakes: the Landers sequence

262 In this section we test the hypothesis of the space and time independence of MFD, and
263 then we show how the TGRE model works in practice. To do that, we consider the
264 Landers earthquake sequence, which started with a magnitude Mw7.3 event occurred
265 on June 28, 1992, in Southern California. The seismic catalog for such a sequence is
266 rich enough to allow a statistically significant data-model comparison. Furthermore,
267 the fault segment that generates the initial earthquake is well-defined in this case, as
268 a detailed mapping of the slip distribution is available: in our analysis we focus on the
269 fault segments that certainly slipped during the Mw7.3 event, as shown in Madden and
270 Pollard (2012) and hereafter called “Landers fault”.

271 Seismic data for the analysis have been taken from the online available Uniform Cal-
272 ifornia Earthquake Rupture Forecast, version 3 (UCERF3) earthquake catalog, which
273 covers the entire California Region from July 1769 to April 2010 and includes events
274 with $\text{mag} \geq 4$ before 1894 and $\text{mag} \geq 2.5$ after this year (Field et al. (2013)). The data
275 relative to the Landers fault have instead been taken from the California Reference
276 Fault Parameter Database (CRFPD)-UCERF2 system, that is easily accessible online
277 (Field et al. (2009)) and does not present substantial differences with respect to the
278 UCERF3 regarding the faults involved by the Landers rupture. For the websites, see
279 “Data and Resources”.

280 In particular, in this application we test whether the MFDs inside and outside the
281 rupture that generates the Landers earthquake come from the same distribution, as it
282 would be expected in the case of space-time independence. Then, we apply the TGRE
283 model to the on-rupture earthquakes, and we quantify the difference of the reliability

of the TGR and TGRE models through the log-likelihood ratio test. The red stripe in panels *a*) of figures from 5 to 8 shows the rupture on the Landers fault. The stripe has a thickness of about 10 km (considering ± 5 km around the latitude of each segment fault point). The analysis is conducted in the following four time intervals: 29 June - 6 July 1992, 29 June - 29 July 1992, 29 June - 29 September 1992, 29 June 1992 - 29 June 1993, that is, respectively 1 week, 1 month, 3 months and 1 year since the day after the Mw7.3 resetting event.

Setting parameters and assumptions

The first step is to define \mathcal{A} , which sets the spatial resolution of the analysis. We consider the case in which \mathcal{A} covers the whole fault rupture of the Mw7.3 earthquake (red stripes in panels *a*) of figures from 5 to 8). For this tutorial application we set the parameters of the TGRE model as follows.

- i) M_c^* corresponds to $m_c^* = 7.59$, as proposed in Kagan et al. (2010) for active continents.
- ii) After the resetting Landers earthquake, no other resetting earthquake occurred in \mathcal{A} in the time interval considered, therefore t_0 corresponds to June 28, 1992.
- iii) $M_{c,0}^*$ is estimated through a grid search; specifically, we search the $m_{c,0}^*$ in the set $[4, 4.1, \dots, 6]$ which maximizes the likelihood ratio in favour of TGRE in the first week of data. As shown in Fig. 9, we find $m_{c,0}^* = 4.3$. Of course, more sophisticated procedures to estimate $M_{c,0}^*$ are possible, but we argue that the results are stable for reasonable variations of this parameter. In particular, the log-likelihood ratio remains well above zero (TGRE explains the data better than

306 TGR) for $4.1 \leq m_{c,0}^* \leq 4.8$. Then, in Table 1 we show also that the $M_{c,0}^*$ estimated
 307 in the first week of data brings to a superiority of TGRE with respect to TGR also
 308 for other time windows (1 month, 3 months, and 1 year) (see section "Results"
 309 for more details).

310 iv) $\nu = \frac{1}{\tau(1-2cov)}$, where the recurrence time $\tau = 250$ years is rescaled accounting for
 311 the covariance coefficient $CoV = 0.3$.

312 The results are illustrated in the next section. To check their stability and the
 313 sensitiveness of the model, besides using different $M_{c,0}^*$, we perform the analysis also
 314 for other possible values of the parameters M_c^* and τ . The details are reported in the
 315 caption of Table 1. We anticipate that the results are not significantly modified, in
 316 agreement with what shown in Fig. 2 previously discussed.

317 Results

318 Results are illustrated in figures from 5 to 8, respectively for 1 week, 1 month, 3 months
 319 and 1 year since the day after the resetting Landers event. The space-time windows in
 320 which the analysis is performed are shown in the map of panels *a*), where the on-rupture
 321 seismicity of \mathcal{A} (red dots) is reported inside the red stripe.

322 In panels *b*) of figures from 5 to 8, we show the results of the null hypothesis of
 323 having the same MFD inside and outside the ruptured area. In particular, we plot the
 324 earthquake cumulative numbers of events inside (in red) and outside (in dark blue) \mathcal{A}
 325 in different time windows. In each of the four temporal intervals, red and dark blue step
 326 functions are clearly different, and the two-samples Kolmogorov-Smirnov test (Massey
 327 (1951)) confirms the rejection of the null hypothesis that the data are drawn from the

328 same continuous distribution, with a p -value much smaller than the 1% significance level
 329 chosen before carrying out the analysis. We stress that these results are completely
 330 independent of the modeling, as they are obtained by considering only earthquake
 331 data. At the same time, these results support the main motivation of this work, i.e.,
 332 empirical data support the hypothesis of different MFDs on- and off-rupture just after
 333 a large shock.

334 Panels $c)$ in all the figures from 5 to 8 show the goodness-of-fit of the TGRE and
 335 TGR models with respect to the earthquake data inside \mathcal{A} . Specifically, we plot the
 336 TGR model in black versus the TGRE one in yellow, orange, green and blue respectively
 337 for 1 week (Fig. 5), 1 month (Fig. 6), 3 months (Fig. 7) and 1 year (Fig. 8) since the
 338 reset. We also show 1000 simulations of 1000 magnitudes each, obtained both with
 339 $m_c^* = 7.59$, that is drawn from a TGR (light gray cones), and with the new corner
 340 magnitudes $m_c(E)$ obtained for the TGRE model (light yellow, orange, green and blue
 341 cones for the four temporal intervals considered). Results show that within one week
 342 since the Landers earthquake, the TGRE corner seismic moment is reduced to a value
 343 $\sim M_{c,0}^*$ corresponding to the minimum energy, and after that it increases with the
 344 energy reloading process.

345 In all the four cases, the TGRE model gives visually a better fit to earthquake data
 346 than the TGR model: the red step functions representing the recorded magnitudes are
 347 almost completely contained in the non-gray cones, indicating our model's capability
 348 to better reproduce the time evolution of the real seismicity occurred in \mathcal{A} that just
 349 experienced the strong resetting Landers event. We argue that this general observation
 350 is independent from the choice on $M_{c,0}^*$, because of the clear bending in the MFD of

the earthquakes inside \mathcal{A} .

We explore further the suitability of TGRE calculating the likelihood ratio for the nested TGR and TGRE models (King (1998)). The likelihood ratio is a measure of how much the TGRE is supported by the data with respect to TGR. In particular, the log-likelihood function

$$\log L(\theta) = N\beta_k \log M_{min} + \frac{NM_{min} - \sum_{i=1}^N M_i}{\theta} + \sum_{i=1}^N \log \left(\frac{\beta_k}{M_i} + \frac{1}{\theta} \right) - \beta_k \sum_{i=1}^N \log M_{min} \quad (6)$$

is the same for both the models, and it represents the TGRE when $\theta = M_c(E)$, and the TGR when $\theta = M_c^*$. In Table 1 we show the difference $\log L(M_c(E)) - \log L(M_c^*)$ between the two log-likelihoods, computed for the four space-time windows considered above. The results in the first row of Table 1 are relative to the earthquake data used in figures from 5 to 8, panels *c*), i.e., with $m_c^* = 7.59$, $m_{c,0}^* = 4.3$ and $\tau = 250$ years. As anticipated in the previous section, to verify the stability of the results as a function of these parameters, we calculate the likelihood ratio also for different m_c^* and τ (see the first three columns in Table 1); for all these cases, we found that $m_{c,0}^* = 4.3$ maximizes the likelihood ratio in favour of TGRE in the first week of data. The results of this stability test are shown in the rows from the second on. Borrowing the terminology adopted by Kass and Raftery (1995) for the Bayes factor, we may say that the evidence in favour of TGRE with respect to TGR is, most of the times, “substantial” and “strong”. As expected, this evidence lowers only in some cases for a long temporal window considered, but it still remains always > 0 , showing a superiority of TGRE with respect to TGR independently from the parameters. In general, the overall first-increasing-then-decreasing trend of the log-likelihood differences when moving to longer

time periods is what expected, as a trade-off between the number of events and the recharging of the elastic energy of the system.

Finally, we find that the results remain stable also when considering completeness thresholds m_{min} higher than 2.5, or when removing the first few days just after the resetting Mw7.3 event, in which m_{min} may be higher than in the following days. As a matter of fact, any problem in the completeness magnitude should have equally affected the MFD of both events inside and outside \mathcal{A} , leaving the difference between the two distributions unchanged.

Discussion and Conclusions

Basic physical principles and empirical evidence suggest that MFD can vary with space and time. To this purpose, in this paper we have proposed the energy-varying seismic moment-frequency model TGRE for earthquake nucleation, which depends on the elastic energy currently available in an area \mathcal{A} of interest. This model acknowledges the elastic rebound theory and justifies the observation that the largest triggered earthquakes nucleate always outside the fault section which has just generated a large shock. In a different perspective, the model may also describe quantitatively an intermittent criticality state that is tuned by the available elastic energy. In other words, the state of self-organized criticality (SOC) – advocated to explain the power law distribution of the seismic moments at large spatiotemporal scales (Bak and Tang (1989); Sornette and Sornette (1989)) – changes in intermittent criticality when zooming on small space-time windows which have been recently involved by a large earthquake, indicating that a fault system approaches and retreats from a critical state by turns (Ben-Zion et al.

394 (2003); Bowman and Sammis (2004); Bebbington et al. (2010)).

395 The TGRE distribution is obtained as a modification of Kagan’s TGR law, in which
396 the corner seismic moment is a time-varying energy function, i.e., it is linked to the
397 proxy of the amount of energy available in \mathcal{A} . The TGRE model is conceptually simple
398 and it depends on a few parameters: i) the corner seismic moment M_c^* , which is loosely
399 related to the strongest event that may nucleate in \mathcal{A} ; ii) the temporal occurrence of
400 the last large earthquake resetting the elastic energy in \mathcal{A} to a residual value; iii) the
401 rate of the energy recovering, which depends on the recurrence time of the fault(s)
402 involved; iv) $M_{c,0}^*$, which is the minimum value for the corner seismic moment which is
403 achieved after the occurrence of a resetting earthquake in \mathcal{A} . In other words, the TGRE
404 right tail $M_c(E)$ abruptly moves to $M_{c,0}^*$ just after the occurrence of a strong (resetting)
405 event, and then it slowly recovers to the long-term value; in practice, the model inhibits
406 the nucleation of a large triggered earthquake in segments that recently experienced a
407 large shock. An interesting feature of TGRE is that it verifies an invariance condition:
408 as the dimension of the selected space-time window becomes larger, it converges to the
409 TGR law with a limiting corner seismic moment M_c^* .

410 The TGRE has been designed purposely simple (depending on a few clear physical
411 parameters), acknowledging that understandability (and usability) is inversely propor-
412 tional to the complexity of a model. Like for any other model, it contains (more or less
413 explicit) subjective choices, but we think that these choices are less subjective than
414 ignoring the empirical evidence that strong triggered earthquakes do not nucleate in
415 the vicinity of a fault just ruptured by another strong event, like assumed in the (T)GR
416 model. Note that this empirical evidence can be hardly explained by space-time vari-

ability of the b -value of the GR law, which would lower, not inhibit, the triggering of large earthquakes on a fault that has just slipped.

Despite its simplicity, we have shown that TGRE may explain well the statistically significant difference of the MFDs relative to on- and off-rupture seismicity for the Landers sequence, and that the results are stable for possible variations of the parameters. In particular, TGRE outperforms TGR for different values of $m_{c,0}^*$, showing the strongest difference for $m_{c,0}^* = 4.3$. Further studies will be necessary to reduce uncertainties on this value. For now, we just notice that the results seem to indicate that it is more important the fact that we allow the corner seismic moment to vary in space and time, rather than the details about the model's parameters choice. That said, we underline that the TGRE reliability (like for any other model) and the comparison with alternative models (e.g., models based on space-time variations of the b -value) have to be evaluated only through prospective tests. For this model, prospective tests will be carried out in the framework of the ongoing european RISE project, which supports the Collaboratory for the Study of Earthquake Predictability (CSEP) network activities in Europe (for the websites, see “Data and Resources”; (Zecher et al., 2010; Schorlemmer et al., 2018)) .

Finally, we suggest that the implementation of the TGRE may offer some benefits for operational earthquake forecasting (OEF) models, because it overcomes one of the conundrum of the best performing current clustering models (Taroni et al. (2018)), for which the likelihood of a large earthquake is exactly where another large earthquake has just occurred. This conundrum has been also identified as one of the main reasons for the instability of the forecasts produced by the UCERF3-ETAS model, which has to

impose a space-time variability of the MFD to solve the problem (Field et al. (2017b)). At the same time, TGRE may also provide a different explanation of recent empirical evidence relative to variations of the b -value before and after large earthquakes close to faults (Gulia and Wiemer (2019)). In particular, although it is worth remarking that the meaning of the b -value is questionable for a distribution that is not exponential, such as the TGR, if the corner magnitude gets closer to the completeness threshold (even though the slope remains the same), the b -value necessarily increases (Marzocchi et al. (2020)).

More in general, since the use of a proper MFD may have a large impact on the earthquake predictability, we hope that this paper will stimulate further thoughts on this issue.

Data and Resources

The data used in this study are available at <http://www.wgcep.org/ucrf3>, <https://pubs.usgs.gov/of/2013/1165/> and <https://pubs.usgs.gov/of/2007/1437/> (last access, January 2019). Finally, for the RISE and CSEP projects, see respectively www.rise-eu.org and https://scec.usc.edu/scecpedia/CSEP_Working_Group (last access, April 2020).

Acknowledgments

We thank the reviewers for their useful comments and suggestions.

References

- Allen, T. I., and G. P. Hayes (2017). Alternative Rupture-Scaling Relationships for Subduction Interface and Other Offshore Environments, *Bull. Seismol. Soc. Am.* 107(3), 1240–1253, doi: 10.1785/0120160255. URL <https://doi.org/10.1785/0120160255>.
- Bak, P., and C. Tang (1989). Earthquakes as a self-organized critical phenomenon, *J. Geophys. Res. Solid Earth* 94(B11), 15635–15637, doi: 10.1029/JB094iB11p15635. URL <https://agupubs.onlinelibrary.wiley.com/doi/abs/10.1029/JB094iB11p15635>.
- Bateman, H. (1953). *Higher transcendental functions*, Mc Graw-Hill Book Company, Inc.
- Bebbington, M. S., D. S. Harte, and S. C. Jaumé (2010). Repeated Intermittent Earthquake Cycles in the San Francisco Bay Region, *Pure Appl. Geophys.* 167, 801–818, doi: 10.1007/s00024-010-0064-6.
- Ben-Zion, Y., M. Eneva, and Y. Liu (2003). Large earthquake cycles and intermittent criticality on heterogeneous faults due to evolving stress and seismicity, *J. Geophys. Res. Solid Earth* 108(B6), doi: 10.1029/2002JB002121. URL <https://agupubs.onlinelibrary.wiley.com/doi/abs/10.1029/2002JB002121>.
- Bowman, D. D., and C. G. Sammis (2004). Intermittent criticality and the Gutenberg-Richter distribution, *Pure Appl. Geophys.* 161(9), 1945–1956, doi: 10.1007/s00024-004-2541-z. URL <https://doi.org/10.1007/s00024-004-2541-z>.

480 Field, E. H., T. E. Dawson, K. R. Felzer, A. D. Frankel, V. Gupta, T. H. Jor-
481 dan, T. Parsons, M. D. Petersen, R. S. Stein, R. J. Weldon, II, and C. J. Wills
482 (2009). Uniform California Earthquake Rupture Forecast, Version 2 (UCERF2),
483 *Bull. Seismol. Soc. Am.* 99(4), 2053. doi: 10.1785/0120080049. URL [http:](http://dx.doi.org/10.1785/0120080049)
484 [//dx.doi.org/10.1785/0120080049](http://dx.doi.org/10.1785/0120080049).

485 Field, E. H., R. Arrowsmith, G. P. Biasi, P. Bird, T. E. Dawson, K. R. Felzer, D. D.
486 Jackson, K. M. Johnson, T. H. Jordan, C. M. Madugo, A. J. Michael, K. R. Milner,
487 M. T. Page, T. Parsons, P. Powers, B. E. Shaw, W. R. Thatcher, R. J. Weldon, and
488 Y. Zeng (2013). Overview of the Uniform California Earthquake Rupture Forecast
489 Version 3 (UCERF3) Time-Independent Model, *AGU Fall Meeting Abstracts*, art.
490 S51F-04.

491 Field, E. H., T. H. Jordan, M. T. Page, K. R. Milner, B. E. Shaw, T. E. Dawson, G. P.
492 Biasi, T. Parsons, J. L. Hardebeck, A. J. Michael, R. J. Weldon, II, P. M. Powers,
493 K. M. Johnson, Y. Zeng, K. R. Felzer, N. van der Elst, C. Madden, R. Arrowsmith,
494 M. J. Werner, and W. R. Thatcher (2017a). A synoptic view of the Third Uniform
495 California Earthquake Rupture Forecast (UCERF3), *Seismol. Res. Lett.* 88(5), 1259,
496 doi: 10.1785/0220170045. URL [+http://dx.doi.org/10.1785/0220170045](http://dx.doi.org/10.1785/0220170045).

497 Field, E. H., K. R. Milner, J. L. Hardebeck, M. T. Page, N. van der Elst, T. H. Jordan,
498 A. J. Michael, B. E. Shaw, and M. J. Werner (2017b). A spatiotemporal clustering
499 model of the Third Uniform California Earthquake Rupture Forecast (UCERF3-
500 ETAS): Toward an operational earthquake forecast, *Bull. Seismol. Soc. Am.* 107(3),
501 1049, doi: 10.1785/0120160173. URL <http://dx.doi.org/10.1785/0120160173>.

502 Gulia, L., and S. Wiemer (2019). Real-time discrimination of earthquake foreshocks
 503 and aftershocks, *Nature* 574, 193–199, doi: 10.1038/s41586-019-1606-4. URL [https:](https://doi.org/10.1038/s41586-019-1606-4)
 504 [//doi.org/10.1038/s41586-019-1606-4](https://doi.org/10.1038/s41586-019-1606-4).

505 Gutenberg, B., and C. F. Richter (1944). Frequency of earthquakes in California, *Bull.*
 506 *Seismol. Soc. Am.* 34(8), 185–188.

507 Hardebeck, J. L., and T. Okada (2018). Temporal stress changes caused by earth-
 508 quakes: A review, *J. Geophys. Res. Solid Earth* 123(2), 1350–1365, doi: 10.1002/
 509 2017JB014617. URL [https://agupubs.onlinelibrary.wiley.com/doi/abs/10.](https://agupubs.onlinelibrary.wiley.com/doi/abs/10.1002/2017JB014617)
 510 [1002/2017JB014617](https://agupubs.onlinelibrary.wiley.com/doi/abs/10.1002/2017JB014617).

511 Ide, S. and G. C. Beroza (2001). Does apparent stress vary with earthquake size?,
 512 *Geophys. Res. Lett.* 28(17), 3349–3352, doi: 10.1029/2001GL013106. URL [https:](https://agupubs.onlinelibrary.wiley.com/doi/abs/10.1029/2001GL013106)
 513 [//agupubs.onlinelibrary.wiley.com/doi/abs/10.1029/2001GL013106](https://agupubs.onlinelibrary.wiley.com/doi/abs/10.1029/2001GL013106).

514 Jordan, T., Y. Chen, P. Gasparini, R. Madariaga, I. Main, W. Marzocchi, G. Pa-
 515 padopoulos, G. Sobolev, K. Yamaoka, and J. Zschau (2011). Operational earthquake
 516 forecasting: State of knowledge and guidelines for utilization, *Ann. Geophys.* 54, 08,
 517 doi: 10.4401/ag-5350.

518 Kagan, Y. Y. (2002a). Seismic moment distribution revisited: I. Statistical results,
 519 *Geophys. J. Int.* 148(3), 520–541, doi: 10.1046/j.1365-246x.2002.01594.x. URL
 520 <http://dx.doi.org/10.1046/j.1365-246x.2002.01594.x>.

521 Kagan, Y. Y. (2002b). Seismic moment distribution revisited: II. Moment conservation
 522 principle, *Geophys. J. Int.* 149(3), 731–754, doi: 10.1046/j.1365-246X.2002.01671.x.
 523 URL <http://dx.doi.org/10.1046/j.1365-246X.2002.01671.x>.

- 524 Kagan, Y. Y., and F. Schoenberg (2001). Estimation of the upper cutoff parameter
525 for the Tapered Pareto Distribution, *J. Appl. Probab.* 38, 01, doi: 10.1239/jap/
526 1085496599.
- 527 Kagan, Y. Y., P. Bird, and D. D. Jackson (2010). Earthquake Patterns in Diverse
528 Tectonic Zones of the Globe, *Pure Appl. Geophys.* 167, 721–741, doi: 10.1007/
529 s00024-010-0075-3. URL <https://doi.org/10.1007/s00024-010-0075-3>.
- 530 Kanamori, H. (1977). The energy release in great earthquakes, *J. Geophys. Res.*
531 82(20), 2981–2987, doi: 10.1029/JB082i020p02981. URL [https://agupubs.
532 onlinelibrary.wiley.com/doi/abs/10.1029/JB082i020p02981](https://agupubs.onlinelibrary.wiley.com/doi/abs/10.1029/JB082i020p02981).
- 533 Kanamori, H., and E. E. Brodksy (2004). The physics of earthquakes, *Rep. Prog.*
534 *Phys.* 67(8), 1429, doi: 10.1088/0034-4885/67/8/r03. URL [https://iopscience.
535 iop.org/article/10.1088/0034-4885/67/8/R03](https://iopscience.iop.org/article/10.1088/0034-4885/67/8/R03).
- 536 Kass, R. E., and A. E. Raftery (1995). Bayes Factors, *J. Am. Stat. Assoc.* 90(430),
537 773–795, URL <http://www.jstor.org/stable/2291091>.
- 538 King, G. (1998). *Unifying Political Methodology: The Likelihood Theory of Statistical*
539 *Inference*, University of Michigan Press, Ann Arbor, URL [http://www.press.
540 umich.edu/titleDetailDesc.do?id=23784](http://www.press.umich.edu/titleDetailDesc.do?id=23784).
- 541 Madden, E., and D. Pollard (2012). Integration of surface slip and aftershocks to con-
542 strain the 3d structure of faults involved in the M 7.3 Landers earthquake, Southern
543 California, *Bull. Seismol. Soc. Am.* 102, 321–342, doi: 10.1785/0120110073.
- 544 Marsan, D., and Y. J. Tan (2020). Maximum Earthquake Size and Seismicity Rate

545 from an ETAS Model with Slip Budget, *Bull. Seismol. Soc. Am.* 0037–1106, doi:
 546 10.1785/0120190196. URL [+https://doi.org/10.1785/0120190196](https://doi.org/10.1785/0120190196).

547 Marzocchi, W., M. Taroni, and G. Falcone (2017). Earthquake forecasting during the
 548 complex Amatrice-Norcia seismic sequence, *Sci. Adv.* 3(9), doi: 10.1126/sciadv.
 549 1701239. URL <http://advances.sciencemag.org/content/3/9/e1701239>.

550 Marzocchi, W., I. Spassiani, A. Stallone, and M. Taroni (2020). Erratum to: How to
 551 be fooled searching for significant variations of the b-value, *Geophys. J. Int.* 221(1),
 552 351–351, doi: 10.1093/gji/ggaa061. URL <https://doi.org/10.1093/gji/ggaa061>.

553 Massey, F. J. Jr. (1951). The Kolmogorov-Smirnov test for goodness of fit, *J. Am.*
 554 *Stat. Assoc.* 46(253), 68–78, doi: 10.1080/01621459.1951.10500769. URL <https://www.tandfonline.com/doi/abs/10.1080/01621459.1951.10500769>.

556 Michael, A. J., S. K. McBride, J. L. Hardebeck, M. Barall, E. Martinez, M. T. Page,
 557 N. van der Elst, E. H. Field, K. R. Milner, and A. M. Wein (2019). Statistical Seis-
 558 mology and Communication of the USGS Operational Aftershock Forecasts for the
 559 30 November 2018 Mw 7.1 Anchorage, Alaska, Earthquake, *Seismol. Res. Lett.* 91(1),
 560 153–173, doi: 10.1785/0220190196. URL <https://doi.org/10.1785/0220190196>.

561 Omi, T., Y. Ogata, K. Shiomi, B. Enescu, K. Sawazaki, and K. Aihara (2018). Im-
 562 plementation of a real-time system for automatic aftershock forecasting in Japan,
 563 *Seismol. Res. Lett.* 90(1), 242–250.

564 Oth, A., D. Bindi, S. Parolai, and D. Di Giacomo (2010). Earthquake scaling char-
 565 acteristics and the scale-(in)dependence of seismic energy-to-moment ratio: In-
 566 sights from KiK-net data in Japan, *Geophys. Res. Lett.* 37(19), L19304, doi:

10.1029/2010GL044572. URL <https://agupubs.onlinelibrary.wiley.com/doi/abs/10.1029/2010GL044572>

Papazachos, B., E. Scordilis, D. Panagiotopoulos, C. Papazachos, and G. Karakaisis (2004). Global relations between seismic fault parameters and moment magnitude of earthquakes, *Bull. Geol. Soc. Greece* 36(3), 1482–1489, doi: 10.12681/bgsg.16538. URL <https://ejournals.epublishing.ekt.gr/index.php/geosociety/article/view/16538>.

Parsons, T., E. L. Geist, R. Console, and R. Carluccio (2018). Characteristic earthquake magnitude frequency distributions on faults calculated from consensus data in California, *J. Geophys. Res. Solid Earth* 123(12), 10,761–10,784, doi: 10.1029/2018JB016539. URL <https://agupubs.onlinelibrary.wiley.com/doi/abs/10.1029/2018JB016539>.

Reid, H. F. (1911). The elastic-rebound theory of earthquakes, *Univ. Calif. Publ. Bull. Dept. Geol.* 6(19), 413–444, URL <https://ci.nii.ac.jp/naid/10006706254/en/>.

Salisbury, J. B., T. K. Rockwell, T. J. Middleton, and K. W. Hudnut (2012). LiDAR and Field Observations of Slip Distribution for the Most Recent Surface Ruptures along the Central San Jacinto Fault, *Bull. Seismol. Soc. Am.* 102(2), 598–619, doi: 10.1785/0120110068. URL <https://doi.org/10.1785/0120110068>.

Schorlemmer, D., M. Werner, W. Marzocchi, T. Jordan, Y. Ogata, D. Jackson, S. Mak, D. Rhoades, M. Gerstenberger, N. Hirata, M. Liukis, P. Maechling, A. Strader, M. Taroni, S. Wiemer, J. Zechar, and J. Zhuang (2018). The Collaboratory for the Study of Earthquake Predictability: Achievements and Priorities, *Seismol. Res.*

589 *Lett.* 89(4), 1305–1313, doi: 10.1785/0220180053. URL [https://doi.org/10.1785/](https://doi.org/10.1785/0220180053)
590 0220180053.

591 Sieh, K., L. Jones, E. Hauksson, K. Hudnut, D. Eberhart-Phillips, T. Heaton, S. Hough,
592 K. Hutton, H. Kanamori, A. Lilje, S. Lindvall, S. F. McGill, J. Mori, C. Rubin,
593 J. A. Spotila, J. Stock, H. K. Thio, J. Treiman, B. Wernicke, and J. Zachariasen
594 (1993). Near-Field Investigations of the Landers Earthquake Sequence, April to
595 July 1992, *Science* 260(5105), 171–176, doi: 10.1126/science.260.5105.171. URL
596 <http://www.jstor.org/stable/2881298>.

597 Sornette, A., and D. Sornette (1989). Self-organized criticality and earthquakes, *EPL-*
598 *Europhys. Lett.* 9(3), 197–202, doi: 10.1209/0295-5075/9/3/002. URL [https://](https://doi.org/10.1209/0295-5075/9/3/002)
599 doi.org/10.1209/0295-5075/9/3/002.

600 Spassiani, I. (2020). Stability of the Epidemic Type Aftershock Sequence model
601 with Tapered Gutenberg- Richter distributed seismic moments, *Bull. Seismol. Soc.*
602 *Am.* issn 0037-1106, doi: 10.1785/0120200012. URL [https://doi.org/10.1785/](https://doi.org/10.1785/0120200012)
603 0120200012.

604 Stallone, A., and W. Marzocchi (2019). Empirical evaluation of the magnitude-
605 independence assumption, *Geophys. J. Int.* 216(2), 820–839, doi: 10.1093/gji/ggy459.
606 URL <http://dx.doi.org/10.1093/gji/ggy459>.

607 Taroni, M., W. Marzocchi, D. Schorlemmer, M. Werner, S. Wiemer, J. Zechar,
608 L. Heiniger, and F. Euchner (2018). Prospective CSEP Evaluation of 1-Day, 3-Month,
609 and 5-Yr Earthquake Forecasts for Italy, *Seismol. Res. Lett.* 89(4), 1251–1261, doi:
610 10.1785/0220180031. URL <https://doi.org/10.1785/0220180031>.

- 611 Temme, N. M. (1996). *Special functions. An introduction to the classical functions of*
612 *mathematical physics*, John Wiley and Sons Inc., New York, 392 pages.
- 613 van der Elst, N. J., and B. E. Shaw (2015). Larger aftershocks happen farther away:
614 Nonseparability of magnitude and spatial distributions of aftershocks, *Geophys. Res.*
615 *Lett.* 42(14), 5771–5778, doi: 10.1002/2015GL064734. URL [https://agupubs.](https://agupubs.onlinelibrary.wiley.com/doi/abs/10.1002/2015GL064734)
616 [onlinelibrary.wiley.com/doi/abs/10.1002/2015GL064734](https://agupubs.onlinelibrary.wiley.com/doi/abs/10.1002/2015GL064734).
- 617 Vere-Jones, D. (1978). Earthquake prediction - A statistician's view, *J. Phys. Earth* 26
618 (2), 129–146, doi: 10.4294/jpe1952.26.129.
- 619 Vere-Jones, D. (1988) On the variance properties of the stress release models, *Aust.*
620 *J. Stat.* 30A(1), 123–135, doi: 10.1111/j.1467-842X.1988.tb00469.x. URL [http:](http://dx.doi.org/10.1111/j.1467-842X.1988.tb00469.x)
621 [//dx.doi.org/10.1111/j.1467-842X.1988.tb00469.x](http://dx.doi.org/10.1111/j.1467-842X.1988.tb00469.x).
- 622 Wang, A.-L., D. Vere-Jones, and X. Zheng (1991). Simulation and estimation proce-
623 dures for stress release model, In M. J. Beckmann, M. N. Gopalan, and R. Sub-
624 ramanian, editors, *Stochastic Processes and their Applications*, pages 11–27, Berlin,
625 Heidelberg. Springer Berlin Heidelberg. ISBN 978-3-642-58201-1.
- 626 Wells, D. L., and K. J. Coppersmith (1994). New empirical relationships among mag-
627 nitude, rupture length, rupture width, rupture area, and surface displacement, *Bull.*
628 *Seismol. Soc. Am.* 84(4), 974.
- 629 Xiaogu, Z., and D. Vere-Jones (1994). Further applications of the stochastic stress
630 release model to historical earthquake data, *Tectonophysics* 229(1), 101 – 121, doi:
631 [https://doi.org/10.1016/0040-1951\(94\)90007-8](https://doi.org/10.1016/0040-1951(94)90007-8). URL [http://www.sciencedirect.](http://www.sciencedirect.com/science/article/pii/0040195194900078)
632 [com/science/article/pii/0040195194900078](http://www.sciencedirect.com/science/article/pii/0040195194900078).

633 Zechar, J. D., Schorlemmer, D., M. Liukis, J. Yu, F. Euchner, P. J. Maechling, and
 634 T. H. Jordan (2010). The Collaboratory for the Study of Earthquake Predictability
 635 perspective on computational earthquake science, *Concurr. Comp.-Pract. E.* 22(12),
 636 1836–1847, doi: 10.1002/cpe.1519. URL [https://onlinelibrary.wiley.com/doi/](https://onlinelibrary.wiley.com/doi/abs/10.1002/cpe.1519)
 637 [abs/10.1002/cpe.1519](https://onlinelibrary.wiley.com/doi/abs/10.1002/cpe.1519).

638 Zheng, X.-G., and D. Vere-Jones (1991). Application of stress release models to his-
 639 torical earthquakes from North China, *Pure Appl. Geophys.* 135(4), 559–576, doi:
 640 10.1007/BF01772406. URL <https://doi.org/10.1007/BF01772406>.

641 Zhuang, J., M. Werner, S. Hainzl, D. Harte, and S. Zhou (2012). Basic models of
 642 seismicity: Temporal models, *CORSSA*, 33.

643 Zöller, G., M. Holschneider, and S. Hainzl (2013). The Maximum Earthquake Magni-
 644 tude in a Time Horizon: Theory and Case Studies, *Bull. Seismol. Soc. Am.* 103(2A),
 645 860–875, doi: 10.1785/0120120013 URL <https://doi.org/10.1785/0120120013>.

Authors' mailing address

646

Spassiani Ilaria (corresponding author)

647

ilaria.spassiani@ingv.it

648

Istituto Nazionale di Geofisica e Vulcanologia (INGV)

649

Via di Vigna Murata 605, 00143, Roma, Italy

650

651

Marzocchi Warner

652

warner.marzocchi@unina.it

653

University of Naples, Federico II

654

Dept. of Earth, Environmental, and Resources Sciences

655

Complesso di Monte Sant'Angelo, Via Cupa Nuova Cintia, 21

656

80126 Napoli, Italy

Table 1: Difference between TGRE and TGR log-likelihoods in bold, and $m_c(E)$ values in brackets.

		1 week	1 month	3 months	1 year	
$m_c^* = 7.59^{\text{a}}$	$\tau = 250 \text{ y.}^{\text{e}}$	$m_{c,0}^* = 4.3$	3.16 (4.301)	3.51 (4.32)	2.76 (4.43)	1.04 (4.96)
$m_c^* = 7.53^{\text{b}}$	$\tau = 100 \text{ y.}^{\text{f}}$	$m_{c,0}^* = 4.3$	3.15 (4.305)	3.36 (4.38)	1.85 (4.69)	0.26 (5.4)
$m_c^* = 7.5^{\text{c}}$	$\tau = 1000 \text{ y.}^{\text{g}}$	$m_{c,0}^* = 4.3$	3.16 (4.3)	3.53 (4.301)	2.65 (4.31)	2.62 (4.4)
$m_c^* = 8.0^{\text{d}}$	$\tau = 500 \text{ y.}^{\text{h}}$	$m_{c,0}^* = 4.3$	3.16 (4.301)	3.51 (4.32)	2.75 (4.43)	1.02 (4.96)

^a $m_c^* = 7.59$ as in Kagan et al. (2010).^c $m_c^* = 7.5$ like for S. Jacinto fault (Salisbury et al. (2012)).^b $m_c^* = 7.53$ by Wells and Coppersmith (1994)'s relations.^d $m_c^* = 8$ close to that for Northern S. Andreas fault.^e $\tau = 250$ like for Northern S. Andreas fault.^g $\tau = 1000$ as in Sieh et al. (1993).^f $\tau = 100$ like for S. Jacinto fault.^h $\tau = 500$ close to a mean value.

Tables

List of figure captions

Fig. 1: Time-varying corner seismic moment $M_c(E) = M_{c,0}^* + (M_c^* - M_{c,0}^*) [\nu(t - t_0)]^2$ as a function of the elapsed time $t - t_0$ between the event (t, M) and the resetting one (t_0, M_0) . Panels *a*), *b*) and *c*) are obtained respectively for: fixed $(M_c^*, M_{c,0}^*)$ – varying ν , fixed $(\nu, M_{c,0}^*)$ – varying M_c^* , fixed (ν, M_c^*) – varying $M_{c,0}^*$. The latter is obtained for a shorter $t - t_0$ interval, because here the differences of the corner seismic moment function can be appreciated: $M_c(E)$ substantially would not change over a longer temporal interval, being M_c^* predominant over $M_{c,0}^*$. Magnitude values are shown in place of seismic moments for an easier interpretation of the figure.

Fig. 2: Surface plots of the time-varying corner seismic moment $M_c(E) = M_{c,0}^* + (M_c^* - M_{c,0}^*) [\nu(t - t_0)]^2$ as a function of the time elapsed since the reset $t - t_0$ and: the parameter ν with fixed M_c^* in the first column panels, viceversa in the second column. The minimum corner seismic moment is set at $m_{c,0}^* = 4.5$ in each panel.

Fig. 3: Survival function of the TGRE model for several values of the available energy (corner seismic moment), corresponding to the $M_c(E)$ indicated in the legend, in a log-log scale.

Fig. 4: TGRE branching ratio (5) versus its time-varying corner seismic moment, for several values of the difference $\beta_k - \alpha_k$.

Fig. 5: TGR vs TGRE analysis relative to the considered area \mathcal{A} , covering the Landers

680 segment fault, as shown in panel *a*) (the colored lines with circles represent the nearby
 681 segment faults). The temporal interval here is 29 June 1992 - 6 July 1992, that is,
 682 within 1 week since the day after the Landers resetting earthquake. The number of
 683 events contained in this spatiotemporal window is 437 (red dots in panel *a*)). Panel *b*)
 684 contains the earthquake cumulative numbers of events inside \mathcal{A} (in red), and outside
 685 it (in dark blue). Finally, in panel *c*) we compare the fit to the data of the TGR model
 686 in black, and the TGRE model in yellow, obtained respectively with $m_c^* = 7.59$ and
 687 $m_c(E) = 4.301$ (the latter derived from equation (2) with $\alpha = 2$). These corner mag-
 688 nitudes are used also to obtain 1000 simulations of 1000 TGR- and TGRE- distributed
 689 seismic moments, respectively, which are plotted as light gray and light yellow cones.
 690 The data (red step functions) almost completely fall into the TGRE cone. Magnitude
 691 values are shown in place of seismic moments for an easier interpretation.

692

693 **Fig. 6:** The same as Fig. 5, but relative to the temporal interval 29 June 1992 -
 694 29 July 1992, that is, within 1 month since the day after the Landers resetting earth-
 695 quake. The number of events contained in this spatiotemporal window is 739. The
 696 color used for the TGRE model is orange, and $m_c(E) = 4.32$.

697

698 **Fig. 7:** The same as Fig. 5, but relative to the temporal interval 29 June 1992 -
 699 29 September 1992, that is, within 3 months since the day after the Landers resetting
 700 earthquake. The number of events contained in this spatiotemporal window is 926.
 701 The color used for the TGRE model is green, and $m_c(E) = 4.43$.

702

703 **Fig. 8:** The same as Fig. 5, but relative to the temporal interval 29 June 1992 -
704 29 June 1993, that is, within 1 year since the day after the Landers earthquake. The
705 number of events contained in this spatiotemporal window is 1120. The color used for
706 the TGRE model is blue, and $m_c(E) = 4.96$.

707

708 **Fig. 9:** Difference between TGRE and TGR log-likelihoods versus the minimum mag-
709 nitude $m_{c,0}^*$ achieved after the reset.

Figures

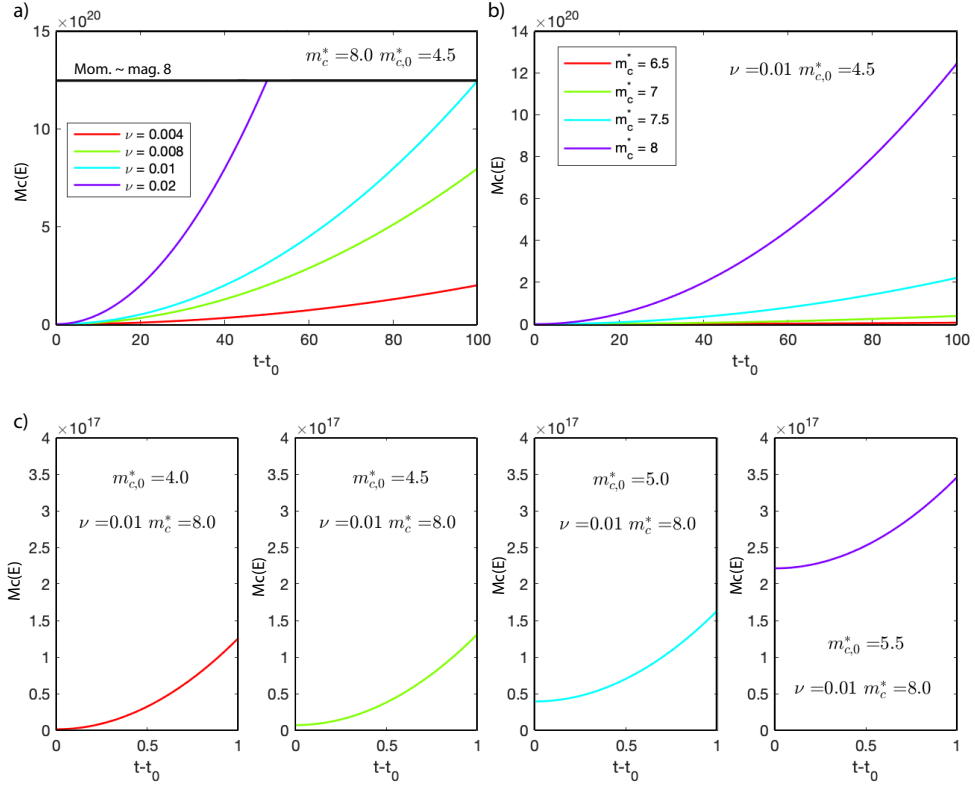


Figure 1: Time-varying corner seismic moment $M_c(E) = M_{c,0}^* + (M_c^* - M_{c,0}^*) [\nu(t - t_0)]^2$ as a function of the elapsed time $t-t_0$ between the event (t, M) and the resetting one (t_0, M_0) . Panels a), b) and c) are obtained respectively for: fixed $(M_c^*, M_{c,0}^*)$ – varying ν , fixed $(\nu, M_{c,0}^*)$ – varying M_c^* , fixed (ν, M_c^*) – varying $M_{c,0}^*$. The latter is obtained for a shorter $t-t_0$ interval, because here the differences of the corner seismic moment function can be appreciated: $M_c(E)$ substantially would not change over a longer temporal interval, being M_c^* predominant over $M_{c,0}^*$. Magnitude values are shown in place of seismic moments for an easier interpretation of the figure.

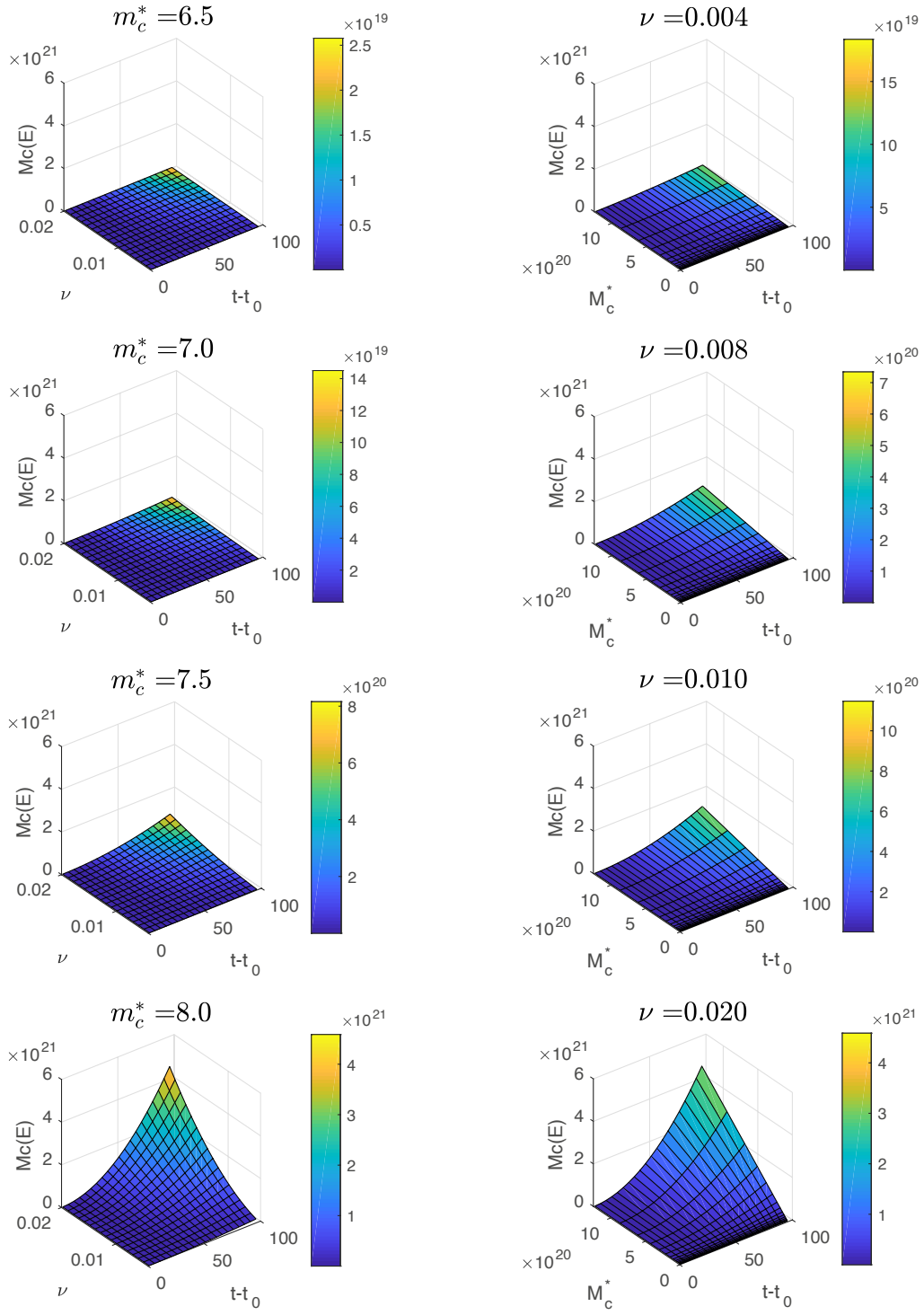


Figure 2: Surface plots of the time-varying corner seismic moment $M_c(E) = M_{c,0}^* + (M_c^* - M_{c,0}^*) [\nu(t - t_0)]^2$ as a function of the time elapsed since the reset $t - t_0$ and: the parameter ν with fixed M_c^* in the first column panels, viceversa in the second column. The minimum corner seismic moment is set at $m_{c,0}^* = 4.5$ in each panel.

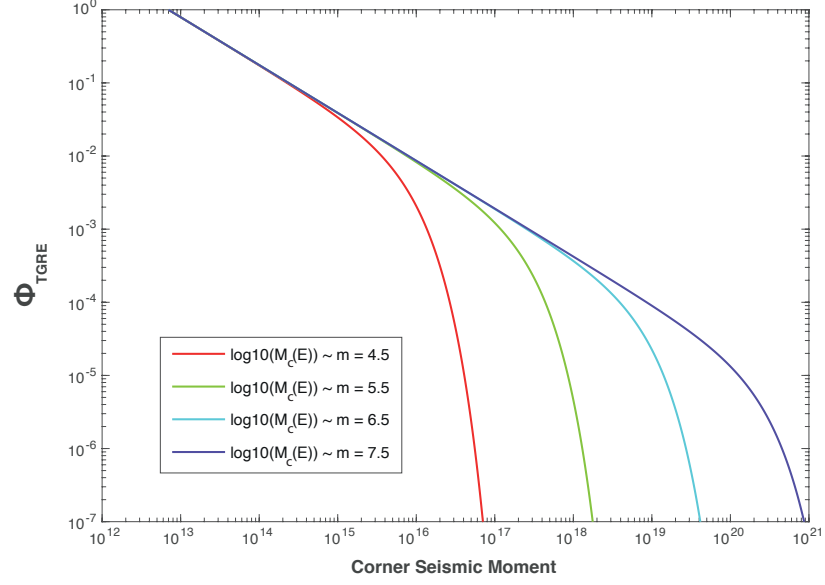


Figure 3: Survival function of the TGRE model for several values of the available energy (corner seismic moment), corresponding to the $M_c(E)$ indicated in the legend, in a log-log scale.

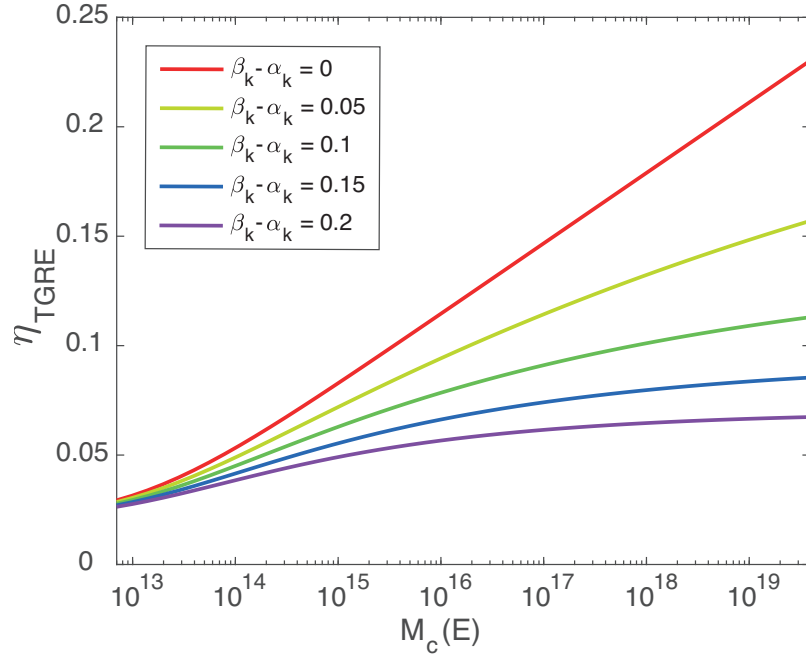


Figure 4: TGRE branching ratio (5) versus its time-varying corner seismic moment, for several values of the difference $\beta_k - \alpha_k$.

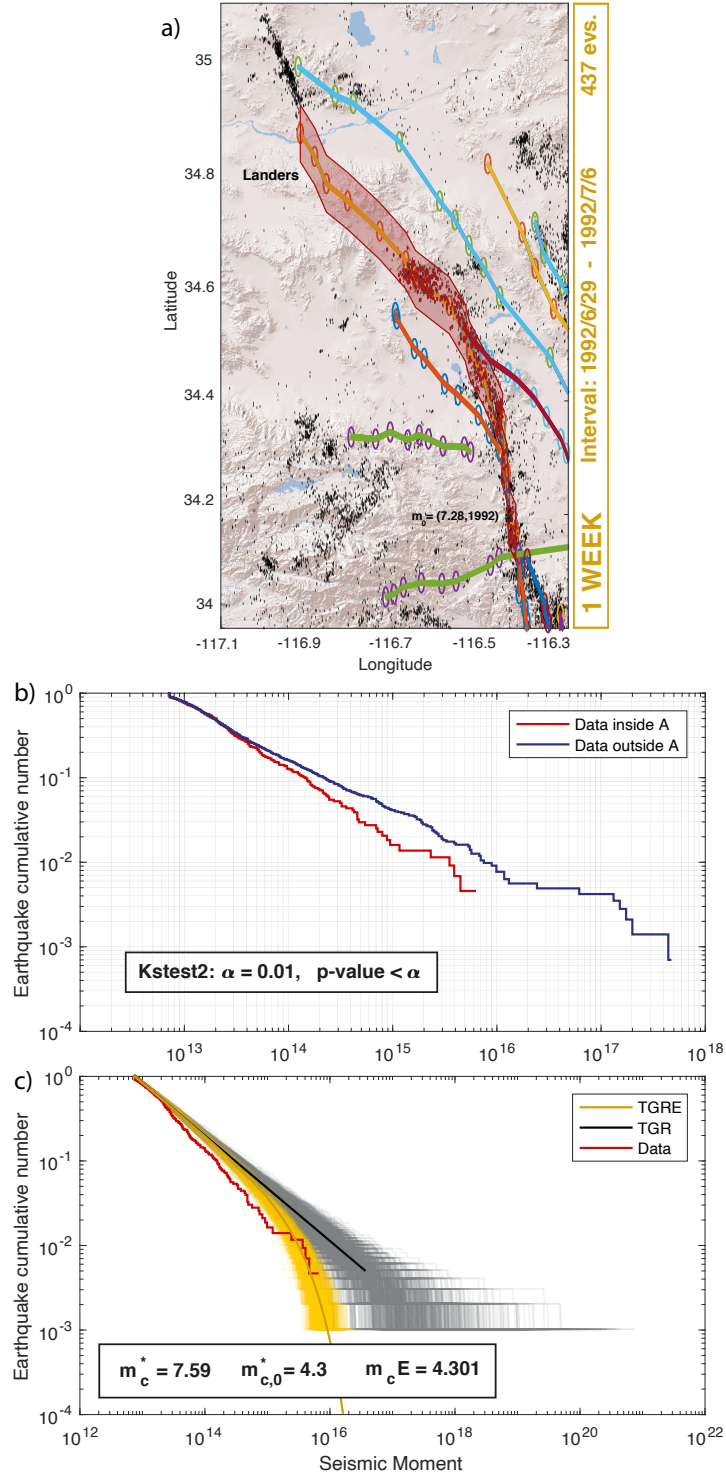


Figure 5: TGR vs TGRE analysis relative to the considered area \mathcal{A} , covering the Landers segment fault, as shown in panel a) (the colored lines with circles represent the nearby segment faults). The temporal interval here is 29 June 1992 - 6 July 1992, that is, within 1 week since the day after the Landers resetting earthquake. The number of events contained in this spatiotemporal window is 437 (red dots in panel a)). Panel b) contains the earthquake cumulative numbers of events inside \mathcal{A} (in red), and outside it (in dark blue). Finally, in panel c) we compare the fit to the data of the TGR model in black, and the TGRE model in yellow, obtained respectively with $m_c^* = 7.59$ and $m_c(E) = 4.301$ (the latter derived from equation (2) with $\alpha = 2$). These corner magnitudes are used also to obtain 1000 simulations of 1000 TGR- and TGRE- distributed seismic moments, respectively, which are plotted as light gray and light yellow cones. The data (red step functions) almost completely fall into the TGRE cone. Magnitude values are shown in place of seismic moments for an easier interpretation.

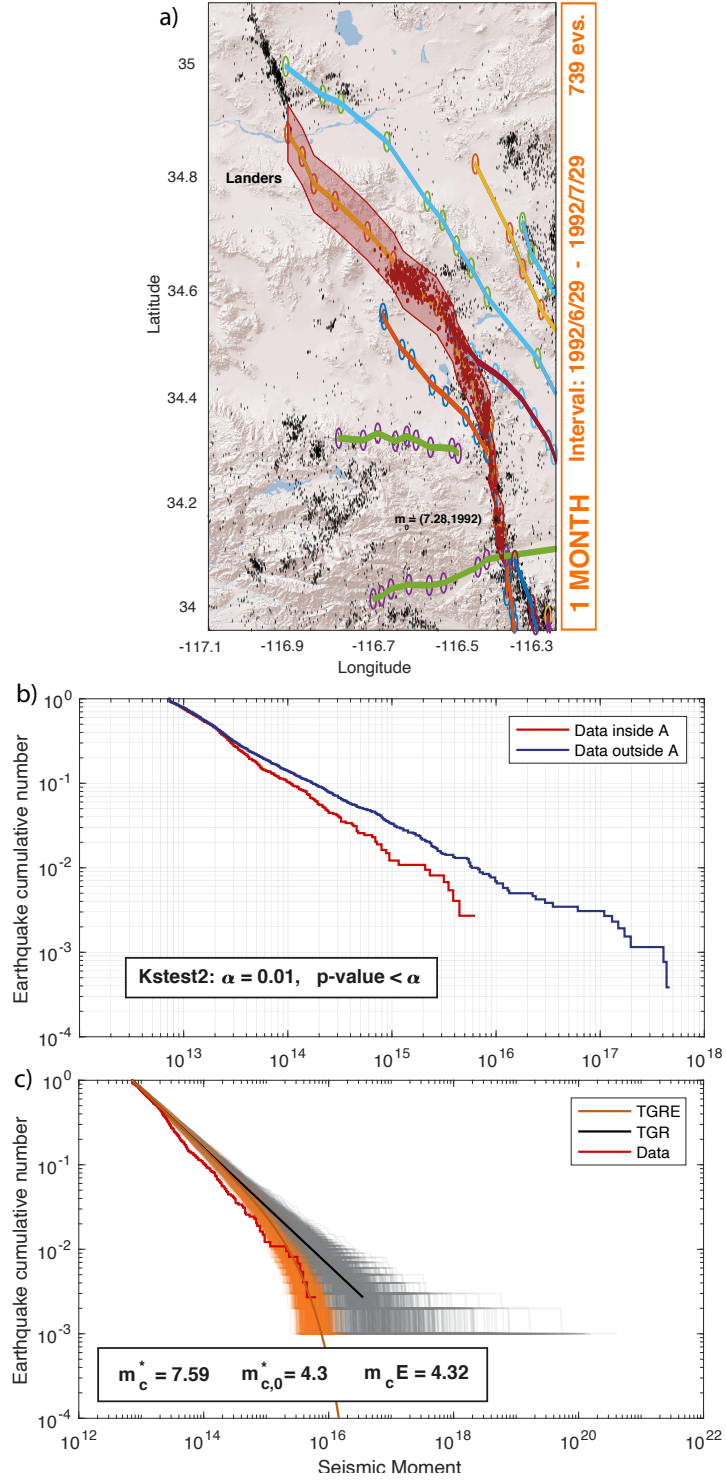


Figure 6: The same as Fig. 5, but relative to the temporal interval 29 June 1992 - 29 July 1992, that is, within 1 month since the day after the Landers resetting earthquake. The number of events contained in this spatiotemporal window is 739. The color used for the TGRE model is orange, and $m_c(E) = 4.32$.

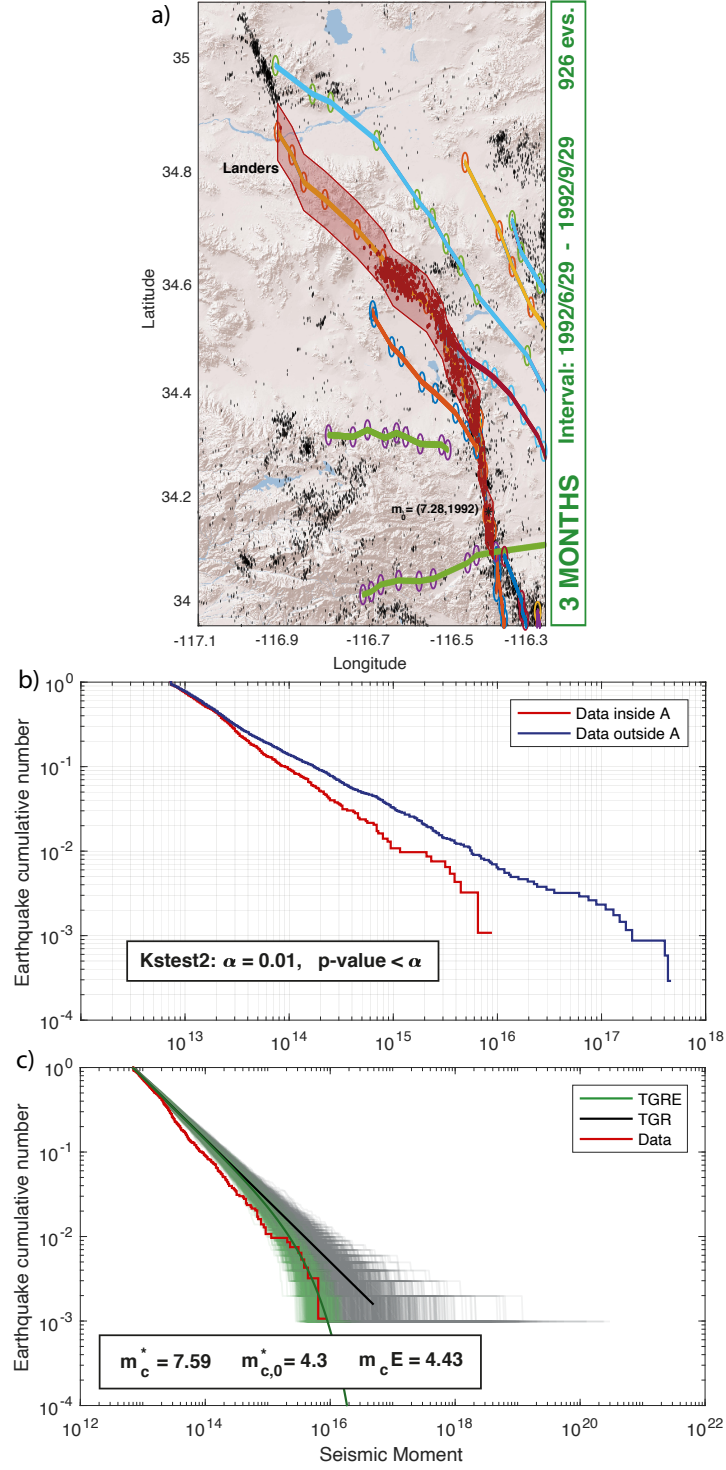


Figure 7: The same as Fig. 5, but relative to the temporal interval 29 June 1992 - 29 September 1992, that is, within 3 months since the day after the Landers resetting earthquake. The number of events contained in this spatiotemporal window is 926. The color used for the TGRE model is green, and $m_c(E) = 4.43$.

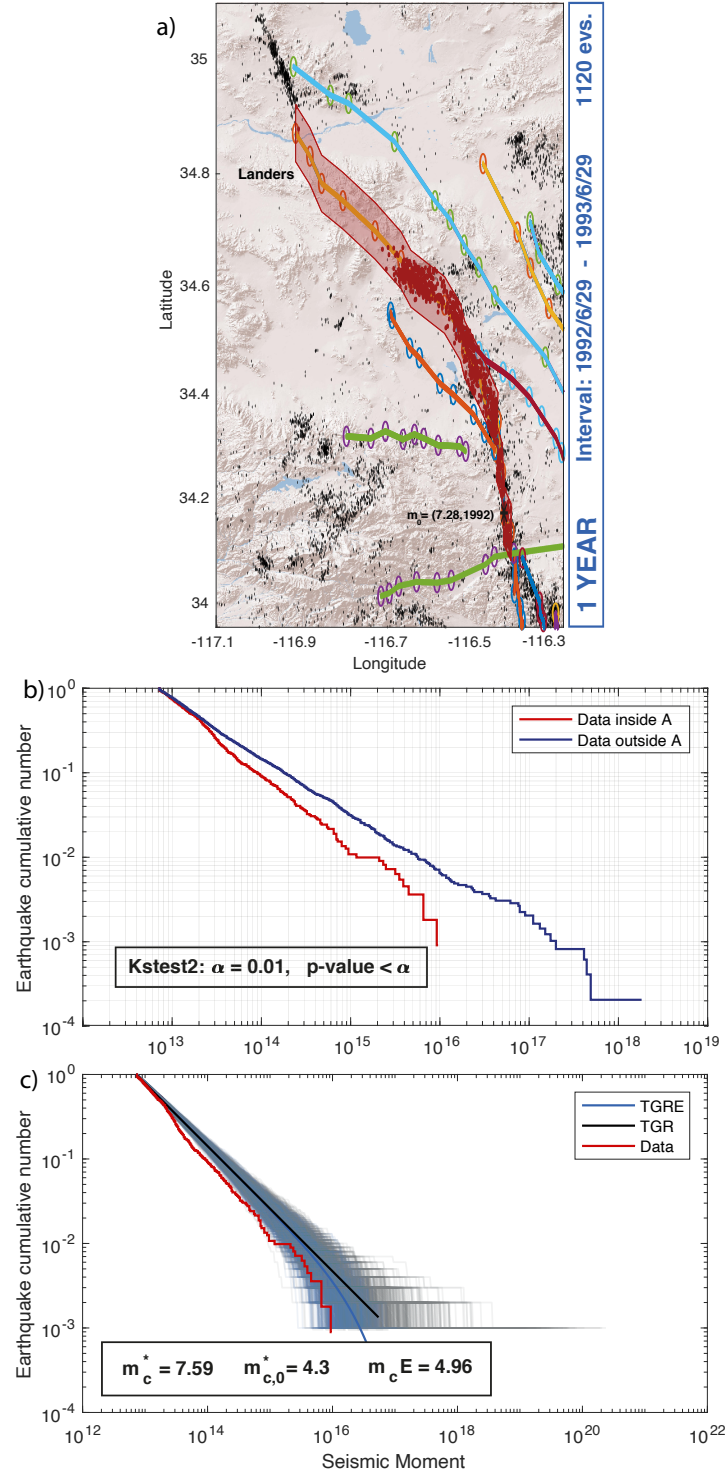


Figure 8: The same as Fig. 5, but relative to the temporal interval 29 June 1992 - 29 June 1993, that is, within 1 year since the day after the Landers earthquake. The number of events contained in this spatiotemporal window is 1120. The color used for the TGRE model is blue, and $m_c(E) = 4.96$.

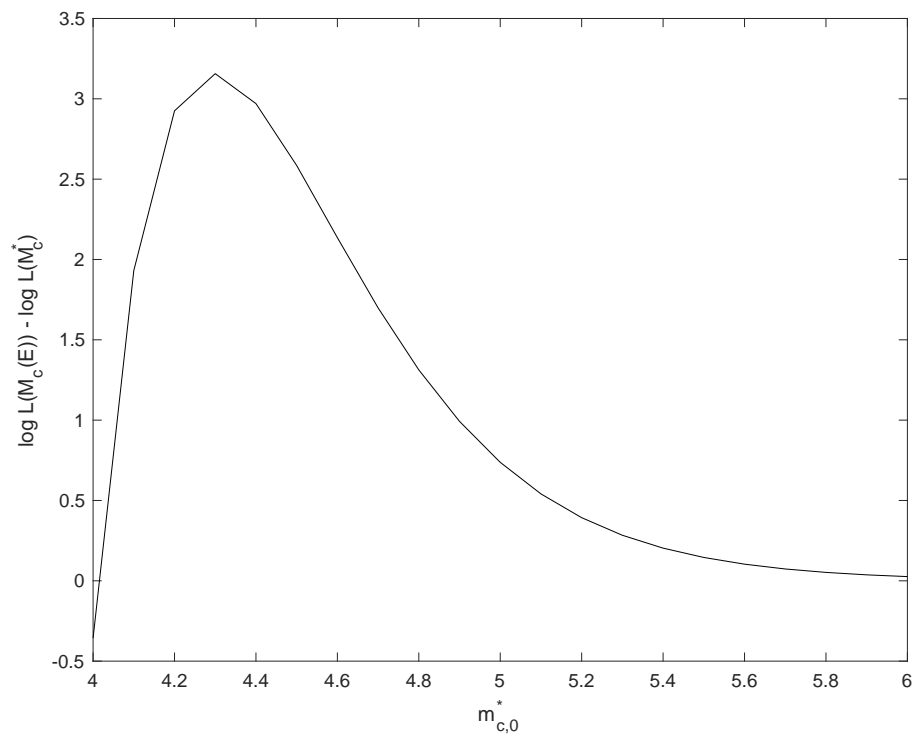


Figure 9: Difference between TGRE and TGR log-likelihoods versus the minimum magnitude $m_{c,0}^*$ achieved after the reset.